CONF-970164--1
UCRL-JC-125099
PREPRINT

Superplastic Deformation in Two Microduplex Stainless Steels

D. R. Lesuer
T. G. Nieh
C. K. Syn
E. M. Taleff

This paper was prepared for submittal to the
International Conference on Superplasticity of Advanced Materials
Bangalore, India
January 29-31, 1997

September 1, 1996

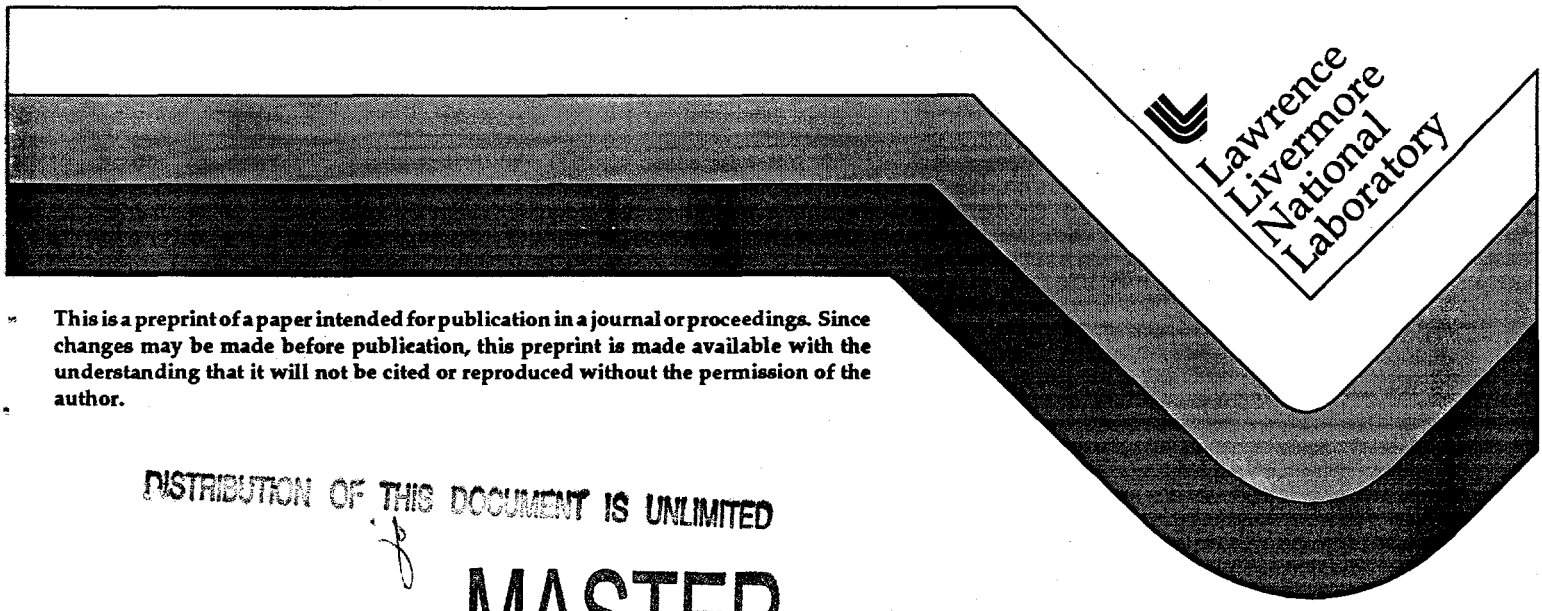

SUPERPLASTIC DEFORMATION IN TWO MICRODUPLEX STAINLESS STEELS

D.R. Lesuer[1], T.G. Nieh[1], C.K. Syn[1], and E.M. Taleff[2]

[1] Lawrence Livermore National Laboratory, Livermore, Califormia, USA
[2] The University of Texas at Austin, Austin, Texas, USA

ABSTRACT

The deformation behavior and mechanisms of superplastic flow in two microduplex stainless steels have been studied at ~$0.7T_m$. The two steels differed in initial grain size by a factor of 3. Both steels exhibited solute-drag-controlled grain boundary sliding in a high temperature $\gamma+\delta$ phase field. In a lower temperature $\gamma+\sigma$ phase field, the fine-grained steel ($\bar{L} = 5$ μm) exhibited climb-controlled grain boundary sliding and the coarser-grained steel ($\bar{L} = 15$ μm) exhibited solute-drag-controlled slip creep.

INTRODUCTION

The existence of superplasticity in microduplex stainless steels has been known for many years[1]. Despite these early observations and numerous subsequent studies of superplastic deformation in these materials (see for example ref. 2) superplastic, microduplex stainless steels continue to be actively studied. Much of this interest results from the commercial importance of stainless steels as well as an incomplete understanding of the deformation behavior and mechanisms responsible for superplastic flow in these materials. This incomplete understanding results from the complex nature of stainless steels including compositions containing many components (with principal alloying additions of Cr, Ni and Mo), multiple phases (including primary phases of austenite, δ–ferrite and σ phase) as well as phase transformations, recrystallization and grain growth taking place during superplastic deformation.

In this study we examine the influence of composition and microstructure on the superplastic behavior of two microduplex stainless steels. One of the materials is a commercially available stainless steel (SuperDux64) with fine, initial grain size (approximately 5 μm), while the other material (Nitronic 19D) had a slightly different composition and an initial grain size of approximately 15 μm. Both materials contained approximately equal volume fractions of austenite and δ–ferrite at room temperature. At elevated temperature (~$0.7T_m$), the SuperDux64 exhibits superplastic behavior with elongations during constant strain rate deformation of 700% [3]. Its deformation behavior is compared with that of the coarser-grained Nitronic19D. The results have been used to study the deformation mechanisms of these two duplex stainless steels.

MATERIALS

The SuperDux64 alloy was obtained from commercial sources. The microstructure of the as-received material showed that the alloy was highly worked indicating that the final processing steps consisted of cold rolling. The composition, which is given in Table 1, is very similar to the composition of several other alloys that have been reported in the literature [4-7] and characterized as Fe-25Cr-7Ni-3Mo alloys. The

material was tested in the as-received condition, since previous studies have shown that the highest elongations in this material are obtained in the as-cold rolled condition [7]. Previous work[6] has shown that, during an isothermal hold at $0.7T_m$ and subsequent mechanical testing, the severely worked material recrystallizes to produce a microstructure consisting of equiaxed islands of austenite (mean linear intercept grain size approximately 5 μm) in a more or less continuous matrix of δ–ferrite (mean linear intercept grain size approximately 7 μm). A typical microstructure is shown in Fig. 1(a) after a constant strain rate test at 950°C.

Table 1. Compositions of Superdux64 and Nitronic 19D

	Fe	Cr	Ni	Mo	Mn	Si	Cu	N	C
SuperDux 64	balance	24-26	5.5-7.2	3-4					.03
Nitronic 19D	balance	21.3	2.1	.2	4.2	.99	.74	.16	.03

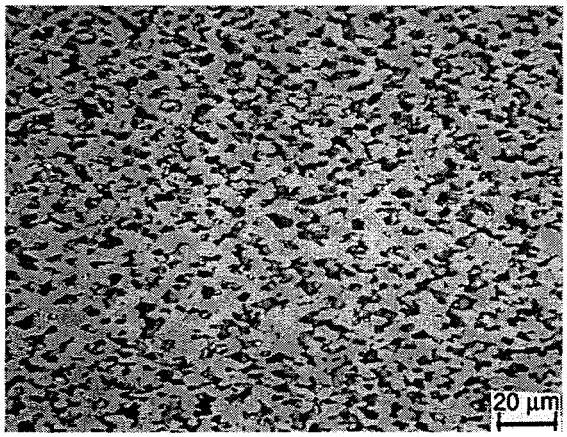

Fig. 1(a). Microstructure of SuperDux64 after tensile testing at 950°C and a constant true strain rate of $2x10^{-4}$ s^{-1}.

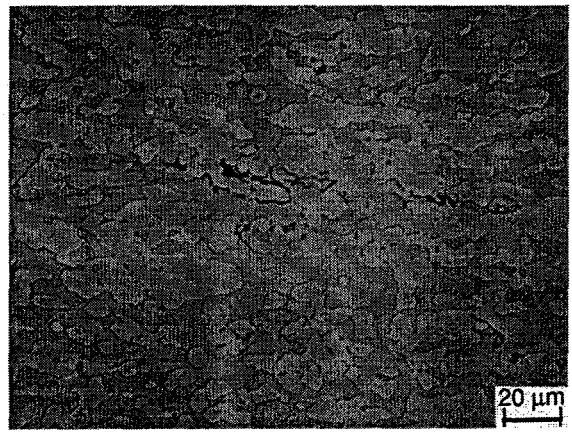

Fig. 1(b). Microstructure of Nitronic 19D after tensile testing at 950°C and a constant true strain rate of $3x10^{-4}$ s^{-1}.

The Nitronic 19D alloy was obtained from Armco Research and Technology in sheet form. The material had the composition given in Table 1 and was hot rolled from 38mm to approximately 3mm (true stain = -2.5) at 1270°C. The as-hot rolled microstructure consisted of elongated islands of austenite in a more-or-less continuous δ–ferrite matrix. Subsequent testing at $0.7T_m$ caused these elongated islands of γ to break up and form roughly equiaxed regions (microstructure had a multi-modal grain size distribution with an average size of 10-20 μm) in a continuous matrix of δ–ferrite. A typical microstructure is shown in Fig. 1(b) after testing at $3x10^{-4}$ s^{-1} and 950°C.

RESULTS AND DISCUSSION

Deformation behavior

Calculations of stress exponent. Data from the strain rate change tests was analyzed according to the well-established constitutive law for creep and superplasticity,

$$\dot{\varepsilon} = K \exp\left(\frac{-Q_c}{RT}\right)\left(\frac{\sigma}{E}\right)^n \qquad (1)$$

where $\dot{\varepsilon}$ is the strain rate, K is a constant (which contains a grain size term for superplastic materials), Q_c is the activation energy for creep, R is the gas constant, T is absolute temperature, σ is the flow stress, E is the dynamic, unrelaxed modulus and n

is the stress exponent. Results were plotted as $\dot{\varepsilon}$-σ/E. Modulus for pure α-Fe as a function of temperature was obtained from the work of Koster [8] and used in data reduction. The elastic modulus for pure α-Fe was used, since elevated temperature, dynamic modulus for Fe-Cr-Ni-Mo alloys was not available. The pure α-Fe values are expected to provide a reasonable representation of the temperature dependence for both phases in the duplex alloy. In fact the data from ref. 8 shows a similar temperature dependence of the modulus for γ-Fe as for α-Fe. Compensating for this temperature dependence is important for the activation energy calculations presented in the next section. Reduced data is shown in Figs 2 and 3. In the low strain rate region, stress exponents have been calculated using a least squares fit of the data to a power law function. The stress exponents calculated in this manner are given in the legend and the predicted $\dot{\varepsilon}$-σ/E response with these stress exponents are shown as straight lines.

	Temperature	n	Microstructure
▲	1050°C	1.12	γ + δ
◆	1000°C	1.43	γ + δ
■	950°C	1.80	γ + σ
●	900°C	2.38	γ + σ

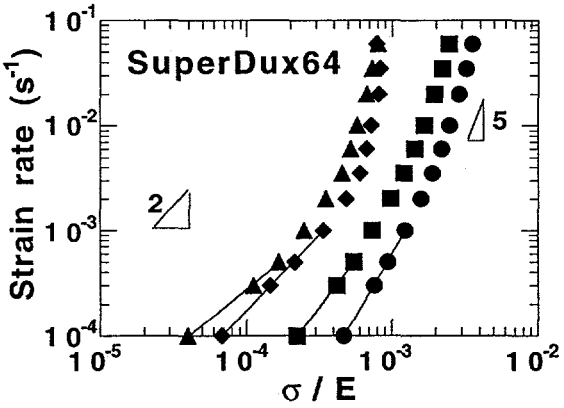

Fig. 2. Strain rate - modulus-compensated stress data for SuperDux64.

	Temperature	n	Microstructure
▲	1050°C	1.80	γ+δ
◆	1000°C	2.26	γ+δ
■	950°C	2.26	γ+σ
●	900°C	2.94	γ+σ

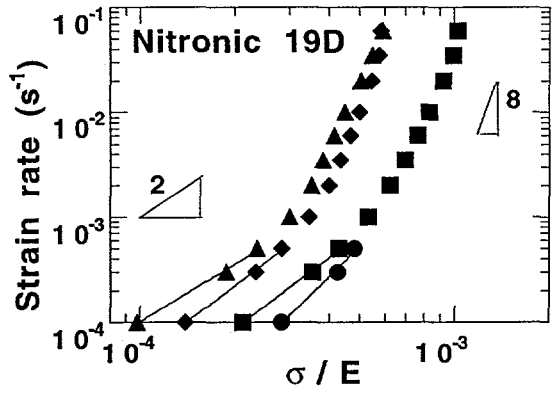

Fig. 3. Strain rate - modulus-compensated stress data for Nitronic 19D.

SuperDux64. Fig. 2 shows the strain rate as a function of modulus-compensated stress for SuperDux64 at 900, 950, 1000 and 1050°C. Examination of Fig. 2 shows the $\dot{\varepsilon}$-σ/E plots group into two sets: one set at 900 and 950°C and another set at 1000 and 1050°C. The reason for this behavior can be understood from the elevated temperautre phase stability studies of Maehara et al on Fe-25Cr-7Ni-3Mo alloys [9]. These investigators showed that, for duplex δ–γ steels with a wide range of compositions, the stable phases are γ and σ in the temperature range of 700-1000°C. In these δ–γ steels, the γ and σ phases form from a euectoid decomposition of the δ phase in this temperature range. In the temperature range 1000-1300°C, the stable phases are δ–γ. Thus the curves at 900 and 950°C are for an equilibrium microstructure of γ and σ phases, whereas the curves at 1000 and 1050°C are for γ and δ phases.

Further examination of Fig. 2 shows that, for both the γ+δ and the γ+σ regions, at strain rates less than 10^{-3} s^{-1}, the stress exponents decrease with increasing temperature. In the γ+δ phase region (1000 and 1050°C), stress exponents are less than two; in fact at 1050°C the stress exponent approaches 1. These low stress exponents suggest that the dominant deformation mechanism in the low strain rate region is grain boundary sliding (GBS) with solute drag as the rate controlling accomodation process. Fukuyo et al [10] proposed this mechanism for superplastic deformation of ultrahigh-carbon steels

containing 10% Al. The model assumes that GBS is accomodated by slip, in which dislocations move sequentially by climb and glide. If dislocations experience strong interactions with solute atoms in solid solution during glide, then the rate-controlling step for deformation can be dislocation glide, as assumed in the model. Accordingly, this mechanism predicts an activation energy for plastic deformation that is equal to the activation energy for solute diffusion in the solid solution. The theory also predicts Newtonian viscous flow (n=1), if solute drag glide is the sole rate-controlling accomodation process. In the UHCS-10Al system, Fukuyo et al [10] observed stress exponents equal to 1.35 and activation energies equal to that for solute diffusion of Al in Fe. This mechanism will be discussed further in the next section, in which activation energies are described.

In the low strain rate, $\gamma+\sigma$ region (900 and 950°C), stress exponents are approximately 2. This stress exponent results, when grain boundary sliding is the dominant deformation mechanism accomodated by dislocation climb. In the high strain rate region, the $\dot{\varepsilon}$-σ/E data in the $\gamma+\delta$ region appears to exhibit a threshold stress. In the $\gamma+\sigma$ region, the data shows a stress exponent of approximately 5, which suggests that deformation is occurring by a slip creep process.

Nitronic19D. The $\dot{\varepsilon}$-σ/E data for Nitronic 19D shown in Fig. 3 has many similarities with the SuperDux64 data. Both materials show an abrupt increase in deformation rate at constant σ/E above 950°C. For Nitronic 19D, this suggests that, as with SuperDux64, the microstructure has changed from $\gamma+\sigma$ at 900 and 950°C to $\gamma+\delta$ at 1000 and 1050°C. Both materials also show a change in n and therefore deformation mechanism at approximately 10^{-3} s^{-1}. At low strain rates in the $\gamma+\delta$ region, the stress exponent is less than 2 at 1050°C and slightly greater than 2 at 1000°C. Thus it appears that at the low strain rates in the $\gamma+\delta$ region (1000 and 1050°C), the deformation mechanism is making a transition to solute-drag-controlled GBS as exhibited by SuperDux64. At low strain rates in the $\gamma+\sigma$ region (900 and 950°C), the stress exponent appears to be approaching 3. This value of the stress exponent is observed, when solute-drag-controlled slip creep is the deformation mechanism. As with solute-drag-controlled GBS, the activation energy for plastic flow with this mechanism is the activation energy for solute diffusion in Fe. At higher strain rates (greater than 10^{-2} s^{-1}), both phase regions show $\dot{\varepsilon}$-σ/E data that has a stress exponent of 8, which suggests that deformation is occuring by a slip creep process (including power law creep and power law breakdown).

Activation Energies and Mechanisms

Calculations of activation energy. Activation energies were evaluated at a constant strain rate of 3×10^{-4} s^{-1}. This strain rate was chosen, because, within a given phase region, deformation mechanisms did not change with increasing temperature (as judged by constant stress exponents). The activation energy was determined from the following expression using the data in Figs. 2 and 3.

$$Q_c = nR \cdot d\ln(\sigma/E)/d(1/T) \qquad (2)$$

A plot of σ/E versus 1/T is shown in Fig. 4 and the activation energies were calculated from the slopes of the lines. The figure clearly shows the transition in activation energy upon going from the $\gamma+\delta$ region to the $\gamma+\sigma$ region. These activation energies, the measured stress exponents and the proposed mechanisms (to be discussed in the next section) are shown in Table II. The activation energies were calculated with an average of the two stress exponents shown in Table II.

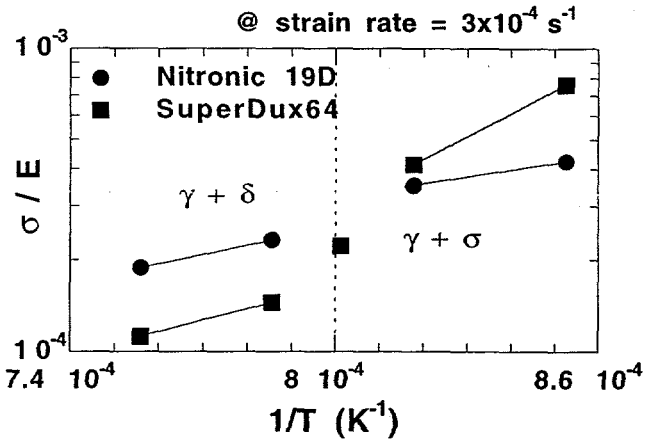

Fig. 4.
σ/E versus 1/T data for SuperDux64 and Nitronic19D.

Table II. Stress Exponents, Activation Energies and Creep Mechanisms

	SuperDux64		Nitronic 19D	
	γ+δ region 1000 + 1050°C	γ+σ region 900 and 950°C	γ+δ region 1000 + 1050°C	γ+σ region 900 and 950°C
n	1.12, 1.43	1.80, 2.38	1.80, 2.26	2.26, 2.94
Q_c (kJ / mol)	92.8	302	122	113
Creep Mechanism	Solute-drag-controlled grain boundary sliding	climb-controlled grain boundary sliding	Solute-drag-controlled grain boundary sliding	Solute-drag-controlled slip creep

SuperDux64. For SuperDux64 in the γ+δ region (1000 and 1050°C), the activation energy for plastic flow equals 92.8 kJ/mol. This value is significantly less than activation energies for Fe self diffusion within the lattice (270 kJ/mol[10]) or along grain boundaries or dislocations (estimated at 163 kJ/mol). Thus the temperature dependence of plastic flow is likely derived from the diffusion of solute atoms within Fe and the activation energy for plastic flow would be equal to the activation energy for solute diffusion in Fe.

Limited diffusion data exists for activation energies of solute diffusion. However, theory provides guidance as to the solute atoms that might be influencing dislocation mobility during solute-drag-controlled GBS. Solutes in solid solution will interact with dislocations and impede their motion due to local strain fields, when solute atoms have a significant size difference relative to the matrix atoms. This size difference can be quantified as a volume size factor, defined as the difference between the atomic volume of solute and solvent normalized by the atomic volume of the solvent. The volume size factors for the major alloying elements in both SuperDux64 and Nitronic 19D relative to the Fe matrix are shown in Table III. For SuperDux64, Mo is soluble in Fe and has a significant size factor; thus this element might be contributing to the rate of dislocation glide during solute-drag-controlled GBS. It is important to note that work by Oikawa et al [11] and Mizukoshi et al [12] on creep mechanisms in Fe-Mo alloys has shown that solute-drag creep can be a significant deformation mechanism in this system. Specifically, the Fe-4.1%Mo alloy (studied by Oikawa et al) exhibited strong solute-drag behavior, while the Fe-1.8%Mo alloy (studied by Mizukoshi et al) exhibited weaker, but significant, solute-drag behavior. Thus Mo, at the concentrations present in the SuperDux64 alloy, can be expected to exhibit solute-drag behavior.

Table III. Volume Size Factors for Alloying Elements in Fe Solid Solution (derived from ref. 13)

Element	Cr	Ni	Mo	Mn	Si	Cu
Volume size factor in Fe	+4.36	+4.65	+27.5	+4.89	-7.88	+17.5

For SuperDux64 in the $\gamma+\sigma$ phase region (900 and 950 °C), the stress exponent is two and the activation energy for plastic deformation is calculated to be 302 kJ/mol. This value is close to the activation energy for self diffusion in Fe (270 kJ/mol). With a stress exponent of 2 and an activation energy equal to that for lattice self diffusion, the mechanism for superplastic flow is generally accepted as GBS accomodated by dislocation climb. Thus in both the $\gamma+\delta$ and the $\gamma+\sigma$ phase regions, the deformation mechanism is GBS; however, the accomodation process changes from dislocation glide (solute drag controlled) to dislocation climb upon going from the $\gamma+\delta$ to the $\gamma+\sigma$ region.

Nitronic 19D. For Nitronic 19D, the activation energies for plastic flow are 122 kJ/mol in the $\gamma+\delta$ region and 113 kJ/mol in the $\gamma+\sigma$ region. As discussed above, both values are less than the activation energies for Fe self diffusion within the lattice, along dislocations or along grain boundaries. Thus the activation energies measured above are likely equal to the activation energy for solute diffusion in Fe. Such an activation energy is consistent with the solute-drag-controlled GBS and solute-drag-controlled slip creep mechanisms proposed for the $\gamma+\delta$ and the $\gamma+\sigma$ regions respectively. Based on the volume size factors in Table III, the solute atoms most likely responsible for solute drag in Nitronic 19D are Cu and Si.

ACKNOWLEDGEMENTS

The authors are indebted to Professor Oleg Sherby for numerous helpful discussions on superplasticity. The authors thank Mr. Rick Gross for mechanical testing and Mr. Jim Ferreira for metallography. The Nitronic 19D used in this investigation was supplied by Armco Research and Technology. This work was performed by the U.S. Department of Energy by Lawrence Livermore National Laboratory under contract No. W-7405-Eng-48.

REFERENCES

1. H. W. Hayden, R. C. Gibson, H. P. Merrick, J. H. Brophy, *Trans. ASM*, 60, 3-14 (1967).
2. Y. Maehara, T. G. Langdon, *Mater. Sci. Eng.*, A128, 1-13 (1990).
3. T. G. Nieh, D. R. Lesuer, C. K. Syn, *Mater. Sci. Eng.*, A202, 43-51 (1995).
4. K. Osada, S. Uekoh, T. Tohge, M. Noda, K. Ebato, *Trans of ISIJ Int'l*, 28, 16-22 (1988).
5. Y. Maehara, *Int'l Conf. Superplasticity in Advanced Materials (ICSAM-91)*, S. Hori, M. Tokizane and N. Furushiros, Eds., (The Japan Soc. for Research on Superplasticity, Osaka, Japan, 1991), pp. 563-568.
6. Y. Maehara, Y. Ohmori, *Metall. Trans.*, 18A, 663-672 (1987).
7. K. Osada, S. Uekoh, K. Ebato, *Trans. ISIJ Int'l*, 27, 713-718 (1987).
8. V. W. Koster, *Z. Metallkunde*, 39, 1-12 (1948).
9. Y. Maehara, Y. Ohmori, T. Murayama, N. Fujino, T. Kunitake, *Metal Sci.*, 17, 541-547 (1983).
10. H. Fukuyo, H. C. Tsai, T. Oyama, O. D. Sherby, *Trans. ISIJ Int'l*, 31, 76-85 (1991).
11. H. Oikawa, M. Saeki, S. Karashima, , Tetsu-to-Hagane, 65, 7, 121-128 (1979).
12. D. Mizukoshi, H. Oikawa, S. Karashima, *Trans. ISIJ Int'l*, 18, 696-701 (1978).
13. H. W. King, *J. Mater. Sci.*, 1, 79-90 (1966).